NUCLEAR INSTRUMENTS AND METHODS 162 (1979) 405-428 ; © NORTH-HOLLAND PUBLISHING CO.

MULTIWIRE PROPORTIONAL CHAMBERS AND DRIFT CHAMBERS

G. CHARPAK and F. SAULI

CERN, Geneva, Switzerland

1. Introduction

Proportional and drift chamber operation depends on the different processes associated with the motion and the interactions of ions and electrons in gases under the influence of electric fields, and the basic laws of the underlying phenomena have been known for decades[1-3]). They have been extensively analysed in the development of many kinds of particle detectors, which have been essential tools used during various phases of nuclear physics research: ionization chambers, Geiger counters, proportional counters, spark chambers[4-7]).

The work undertaken at CERN in 1967 and 1968[8]) brought to light a few essential features of multiwire structures and resulted in very fast development[9]). These structures had previously been used on some rare occasions, but without their most important properties being perceived. It was immediately clear that with the help of the formidable arsenal of modern electronics a new generation of particle detectors was at hand.

Among the early observations that appeared to be significant we may mention that:

- Arrays of anode wires, stretched even at small distances from each other, sandwiched between two cathode surfaces, constitute independent detectors.
- The motion of the positive ions permits the localization of avalanches along the wire by using the pulses induced on appropriate cathodes. This showed that the chambers were a new, adequate tool for low-energy X-rays or neutron imaging[10]).
- The time lag between the ionizing event and the appearance of a pulse could be used for high-accuracy position measurements[10]).
- A spatial resolution of 100 μm was readily obtained by measuring the drift-time in simple structures[11]).

After 10 years of intensive work by many talented groups, and the use of novel ideas, a great variety of gaseous detectors[12]) are now being used in nuclear science, in high-energy physics and in many other fields of applied research[13]).

Various physical phenomena control the properties of these detectors[12]). Among the most important we may mention:

- The energy loss distribution of the radiation being detected. While in most applications no useful information is required from the pulse heights, there are cases of growing importance where it is necessary to have a response proportional to the energy losses: transition radiation detectors, identification of particles in the relativistic rise region, etc.
- The drift of electrons and ions in gases under the influence of moderate electric fields, where they do not experience ionizing collisions.
- The multiplication of electrons in short-range avalanches produced by the very intense fields in the vicinity of the anode wires.
- The propagation of discharges over large distances, mediated mainly by photons emitted by the atoms excited in the avalanche process.
- The electrostatic properties of multiwire structures which control the charge distribution on the different electrodes and the relative intensity of the electric fields[14]).
- The charge distributions induced on the different electrodes by the motion of the liberated ions[15]).

Within the scope of this article we will not detail all these factors and refer the reader instead to the quoted references.

We would rather like to clarify, in a qualitative way, the relations of the most important properties of the detectors to the underlying physical phenomena.

2. The proportional counter

We will shortly summarize here the main properties of single wire proportional counters and refer the reader for more details to some literature on the subject[4,6]).

Such a counter consists of a thin wire stretched at the axis of a conducting cylinder, usually filled with a gas of small electron affinity. The electrons liberated in the gas by an ionizing radiation drift to the positively charged wire and, when reaching its vicinity, they experience inelastic ionizing collisions, giving rise to a multiplicative avalanche. The electrons liberated in the avalanche are collected by the wire, while the positive ions move towards the cathodes. The pulse detected on the wire is mainly produced by the motion of the positive ions. Indeed the signal induced on a collecting electrode is proportional to the potential excursion of the moving charges. The electrons, being produced very close to the wire, experience a small potential drop despite the very high field, while the positive ions have to travel all along the path between the immediate proximity of the anode wire, up to the cathode. This is true in the vast majority of cases, while there are some exceptions for high gain operation as we will see later. The conditions of amplification in multiwire chambers and drift chambers are nearly the same as in single wire counters, however their recent extensive use and the related developments have given rise to a greater variety of gases being used, with a deeper understanding of their properties. Very high gas amplification has been reached without entering into Geiger propagation or sparking, and special shapes of the space–time relations for the drifting electrons have been looked for. More has been learned about the distribution of avalanches around anode wires.

Most of the new chambers use gases at atmospheric pressure, although high pressures have been investigated in relation to an improvement of the spatial accuracy[16]). Low pressures, required for the use of the chambers in detecting heavily ionizing particles, have led to spectacular and surprising results, giving rise to detectors with time resolution well below 1 ns, almost 50 times better than if operated at atmospheric pressure[17]). We will limit our discussion here to chambers working at atmospheric pressure. In these conditions, and in fields around 10^5 V/cm, the mean free path of electrons for ionizing collisions is close to 1 μm and, for gains of the order of 10^5, the maximum radial extension of an avalanche is of the order of 20 μm. At low gains, therefore, a single avalanche does not surround the wire, as generally believed so far. Quantitative measurement of the azimuthal spread of avalanches around the wire have recently been made[18,19]) recording the ion currents at different angles around an anode wire for radiations incident at a given azimuth. As an example, fig. 1 shows the angular distribution of the ions for different amplification factor in a mixture of argon (92.5%), CO_2 (6%) and ethyl alcohol (1.5%); the lateral extension of the avalanche increases with its size, and eventually surrounds the wire at a gain value that depends on the composition.

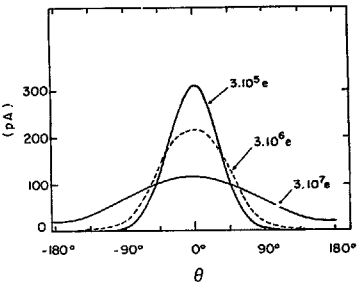

Fig. 1. At moderate multiplication factors, avalanches produced in a cylindrical proportional counter by a localized ionization have a very little spread around the anode wire. The curves show the positive ion current measured for several avalanches as a function of azimuth angle around the anode; an 8 keV X-ray beam (liberating in the gas about 300 electrons) is collimated around $\theta = 0°$. The wire diameter is 20 μm, the gas filling argon–CO_2–ethyl alcohol (92.5–6–1.5)[18]).

Some powerful quenching mixtures have been found where the limit of amplification is mainly set by the space charge and reaches values around 10^7; the density of positive ions in this case grows so high as to cancel the external field stopping any further growth of the avalanche. This is the case for the so-called magic gas[20]) which was very popular at the beginning of the use of multiwire proportional chambers when sensitive amplifiers of low cost were no as cheap and available as now. Recent studies show, however, an interesting feature of this mode of operation[19,21]). Two types of pulses seem to coexist: one corresponding to a propagation of the discharges around the wire, and another to a radial propagation in an interrupted streamer mode. The ultra-violet photons give rise to a string of avalanches just like a streamer in a parallel gap spark chamber, but the string is interrupted in the low field region far from the anode wires. In this case electrons are collected over such a long distance that they experience a large

potential drop and are therefore responsible for most of the fast signal. This is a case where the well accepted idea that in a proportional chamber the pulses are produced by the motion of positive ions only appears wrong. The characteristics of the signal, i.e. large pulse height and fast rise-time, explain why the magic gas is still widely used.

With thick wires, having for instance 100 μm diameter, another peculiar behaviour has been observed, interpreted as a limited Geiger propagation along the anode wire[22]). It originates large and shaped pulses, as in the streamer mode.

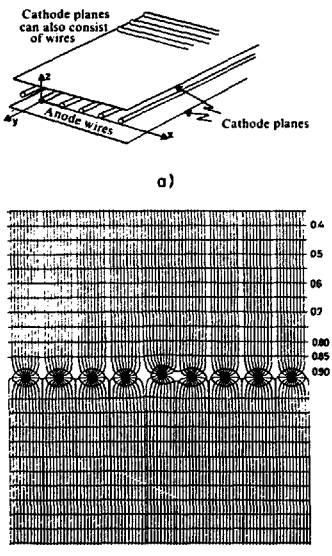

Fig. 2. The multiwire proportional chamber consists of a grid of uniformly spaced thin anode wires, sandwiched between two cathode planes. Cathodes may either consist of uniform conducting foils, or of wire grids (a). The coordinate system used throughout this paper is also shown, as referred to the chamber structure. The origin is centred on an anode wire. When a symmetric difference of potential is applied between anodes and cathodes, an electric field develops as represented in (b) in a plane xz, perpendicular to the anodes. Two main regions of field, leading to the particular behaviour of the counter, can be identified: a region of roughly constant field extending in most of the gap, and a region of rapidly increasing field around the wires where avalanche multiplication occurs. Moreover, low field regions exist between the wires, with some consequences on the collection properties of the chamber[10]).

3. The multiwire proportional chamber

3.1. Generalities

A multiwire proportional chamber (MWPC) usually consists of a plane of equally spaced anode wires, sandwiched between two cathode planes (fig. 2a). The equipotential lines for such a structure (fig. 2b) show three regions of electric field. In the major part of the volume the field is uniform; close to the wire it varies inversely with the distance r to the axis, almost exactly as in a cylindrical counter (fig. 3); and just between the wires there is a small region of very low field. If a particle produces ion pairs in the gas of such a structure, the liberated electrons drift towards the anode wire. Reaching its vicinity, they find the same conditions as in a cylindrical counter: a multiplicative avalanche develops. We find the same variety of amplification processes: an avalanche size proportional to the number of initial electrons for low gains, an amplification saturated by space-charge effects for high gains, a propagation by secondary photons for gases with low quenching properties leading either to a Geiger type propagation along the wires[23]) or to a streamer mode, interrupted or bridging the electrodes and followed by a spark.

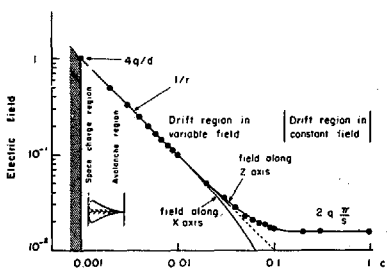

Fig. 3. The electric field strength (on an arbitrary scale) along the z and x directions, as from the definitions of fig. 2. The different field regions are identified in the figure by a short description of the main physical processes occurring[11]).

The motion of the ions liberated in the avalanches controls all the important information that can be extracted from a chamber. This is why a clear qualitative understanding of the mechanism of inducing the positive pulses seems to us a useful preliminary.

3.2. Pulses induced by moving ions in a multiwire structure

Consider a positive charge liberated in the volume of a MWPC. Lines of force connect this charge to the different electrodes. When the charge is close to the anode wire, most of the lines are ending on the wire (fig. 4); as it starts moving away, however, the density of lines reaching the neighbouring anode wires or the cathodes is increasing and pulses of the same sign are induced on all electrodes except the closest anode wire. This is true as long as the ions are not very far from the initial anode wire; it is an essential phenomenon in wire chamber structure and is the very reason for the localizing properties of the wire collecting the electrons from an avalanche: it carries a negative pulse, while all neighbouring wires provide positive signals.

It was at first believed that this was a proof that the avalanche surrounds the wire. It is true that in case of very high amplification, the electrons may propagate around the wire either by diffusion or as a consequence of secondary electrons being ejected by the photons emitted by the excited atoms in the avalanche. However, a cylindrical distribution of ions around the wire is not necessary to justify the near equality of the fast component of the pulse induced on the neighbouring electrodes.

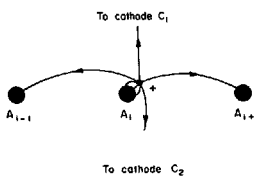

Fig. 4. Schematic illustration of the induced pulses formation in a multiwire chamber. Positive ions, produced around the anode A_i, project lines of force on all surrounding electrodes; at the beginning, the wire A_i itself receives most of them. As ions move away from the wire, both the adjacent wires and the cathodes receive an increasing number of lines of force, resulting in a positive induced charge on all surrounding electrodes irrespective of the direction of motion. When a localized positive charge has drifted far enough from the anode plane, the polarity of the induced signals in some electrodes will eventually invert. Usually, however, only the first fast component of the induction is exploited.

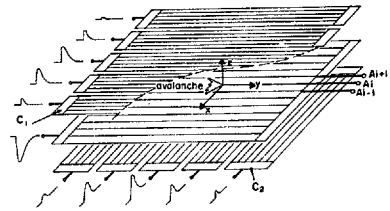

Fig. 5. Principle of localization of avalanches in a multiwire proportional chamber by the method of centre of gravity of the induced charges. Ions leaving the vicinity of an anode wire induce a positive charge distribution on both cathode planes; if these distributions are measured on each event using a convenient stripping of the cathode planes along two perpendicular directions, calculation of their centre of gravity allows both x and y coordinates of the avalanche to be measured[21]).

The relative distributions of the charges induced on the various electrodes carry information; these distributions have been studied in chambers having segmented cathodes, either printed circuit strips or groups of wires, parallel and orthogonal to the anode wires[21]) (fig. 5). The pulses induced on the cathode strips and on the anode wires have been analysed for various conditions of gaseous amplification.

Since the pulses are produced by avalanches very close to the wire, the time lag between the creation of ionization in the gas and the appearance of a pulse is a function of the distance of the ionizing phenomena[8-10]) to the sense wire. It was recognized in the early work on MWPCs that this opens up the possibility of interpolating the positions between wires; however, with a narrow wire spacing, like 2 mm, a fundamental ambiguity appears: it was considered impossible to recognize from which side of the wire the electrons were drifting. This has led to the building of drift structures of various types, designed to overcome the right–left ambiguity and use the drift time to measure position. We will see, however, that recent progress has led to a solution of the ambiguity by a proper use of the wealth of information carried by the different induced pulses.

3.3. A SAMPLE OF IMPORTANT PROPERTIES

To better illustrate the nature of the information that can be extracted from a MWPC, by proper handling of the available signals, we will report here some results obtained at CERN in a small size chamber of the kind illustrated in fig. 5 [21,24]). Under either X-ray or charged particle irradiation, the pulse-height distribution on the cathode strips as well as on the anode plane is recorded and analysed.

It is extremely important to know the spatial distribution of an avalanche and the fluctuations in its extension for a proper understanding of the accuracy limitations connected with the avalanche. Sources of soft X-rays are convenient for this study, since the range of the photoelectrons can be small enough to consider the avalanches as having had a punctual origin. The 1.4 keV Al X-rays and the 5.9 keV X-rays emitted by ^{55}Fe sources are mostly used and the study of the centroid of the induced pulses exhibits very clear properties.

For example, fig. 6 shows the distribution of the centre of gravity for three positions of a collimated 1.4 keV X-ray beam, 200 μm from each other, measured along the direction of the anode wires. The width of the distributions, 35 μm r.m.s., is consistently equal to the range of the photoelectron in the gas: dispersions intrinsic to the avalanche process itself appear therefore to be extremely small.

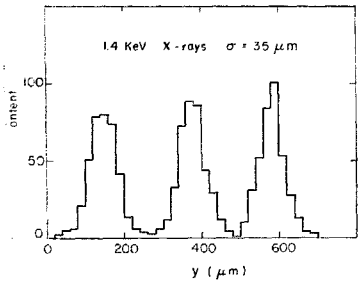

Fig. 6. Precision of localization of a soft (1.4 keV) X-ray beam along the y direction (parallel to the anode wires, see fig. 5) using the method of centre of gravity of the induced pulses. The computed coordinates for three positions of the collimated beam 200 μm apart are represented, showing a localization accuracy of 35 μm r.m.s. This value is rather close to the intrinsic physical limit as imposed by the range in the gas of the produced photoelectron[21]).

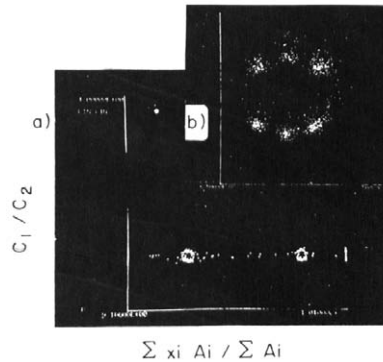

Fig. 7. Localization properties in the plane xz, perpendicular to the anodes, when fully exploiting the information provided by the induced pulses on the cathodes. In both pictures, the horizontal scale represents the measured centre-of-gravity in the x direction, while in the vertical direction the ratio of total pulse heights induced on the two cathodes, or z coordinate, is presented. When uniformly irradiating the chamber with a soft X-ray source, the majority of reconstructed points in this representation cluster in circles centred around the anode wires, with a few events in between corresponding to energy sharing between wires (a). Expanding the scales around one wire, and exposing the chamber to three collimated beams produces the image shown in (b): the three beam positions differ by 500 μm, the middle one being centred on the wire[21]).

Fig. 7a shows instead the distribution of the centroids in a plane orthogonal to the wires, for a uniform irradiation to 5.9 keV X-rays.

In the picture, the abscissa represents the centroid position along the direction perpendicular to the anode wires, the x direction as from fig. 5, and the ordinate the ratio of the pulse heights on the two cathodes. Ring-shaped patterns appear, centred on each anode wire, with a diameter close to 200 μm. This proves that the photoelectrons released in the gas by the X-rays, localized in space, give rise to an avalanche within a very narrow azimuthal spread: this is best illustrated when recording the centroid distributions on three collimated source positions, hitting the anode wire and at 500 μm on each side of it (fig. 7b). It is clearly possible to obtain, with X-ray beams orthogonal to the plane of the chambers, the exact position of the initial photoelectron between the anode wires, by extrapolating back the measured azimuthal position along the corresponding line of force.

With less accurate methods of determining the centroid of the charge, the response is not a ring but a simple point, and for a long time it was considered as a postulate that the ultimate accuracy of wire chambers was the wire distance.

Fig. 8 shows how use of the azimuthal information improves the image quality in the radiography of an object. The position accuracy between wires is around 150 μm, which is a serious progress for 2 mm wire spacing.

When detecting charged particles we usually do not deal with a single avalanche. Because of the large statistical fluctuations in the energy deposit process, we cannot expect to find in this case accuracies as good as for the detection of X-rays. In particular, in the direction perpendicular to the anode wires, electrons produced all along the ionization trail are collected at different azimuthal positions around the anode. Still, an accurate measurement of the centre of gravity in this case shows that events are clustered in two distinct peaks, each corresponding to a definite side of the wire (fig. 9). The peaks overlap in no more than 5% of the events, corresponding to an error of

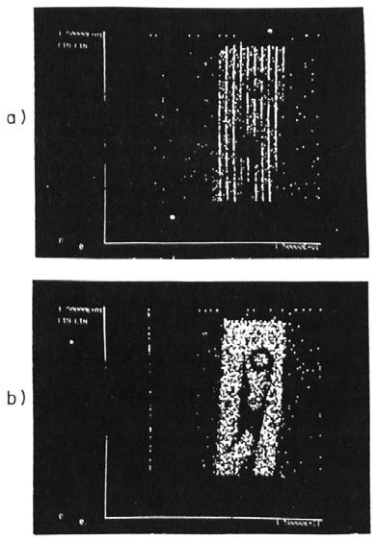

Fig. 8. Absorption radiography of a simple object (a metal clip holding a ring) realized using a bi-dimensional chamber like the one illustrated in fig. 5. In (a) are represented the centres of gravity, directly as computed from the induced charge distribution; the anode wire structure clearly appears. In (b), instead, a continuous response has been obtained taking into account the measured azimuthal angle of the avalanche and correcting correspondingly the value of the coordinate x, perpendicular to the anode wires[24]).

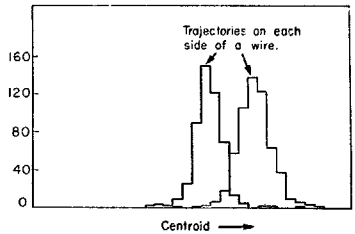

Fig. 9. Right–left separation in a multiwire chamber. For minimum ionizing charged particles orthogonal to the chamber, the centroid of the avalanches corresponding to trajectories on the right and the left of a wire clearly separate, with an overlap in 5% of the cases only corresponding to an error of about 150 μm for the few particles centred on the wires. By measuring the time of the pulses relative to a fast detector, a high accuracy continuous response is also obtained for the coordinate orthogonal to the wires of charged particles[24]).

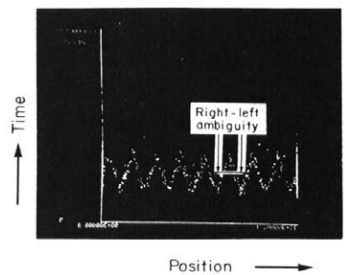

Fig. 10. Space–time correlation in a multiwire proportional chamber. The diagram shows the variation of the time of detection of charged particles as a function of the position of the track relative to the wire. The right–left ambiguity can be lifted by the centroid measurement on cathode strips parallel to the wires, as shown by the previous figure. The horizontal axis shows the measured centre of gravity along the x direction, the scale being defined by the wire spacing (2.5 mm in this case, corresponding to the lowest vertices of the image); the vertical axis represents the time of collection, spanning about a 30 ns interval[24]).

$\sigma = 150\ \mu m$ for those particles close to the wire and giving rise to a right–left ambiguity.

If the time lag of the anode pulse is measured, taking as reference time the passage of the particle as given by a scintillation counter, the display of the time versus position along the x direction shows how easy it is to interpolate between wires (fig. 10). This was not so feasible at the early stage of MWPCs since the ambiguity concerning the side of arrival of the electrons with respect to the anode wires was introducing an error which could be removed only by complicated means.

In the y direction, along the anode wires, the presence of multiple avalanches has a smaller effect on the obtainable accuracy, at least for tracks perpendicular to the chamber; dispersions with about 50 μm r.m.s. have been measured for minimum ionizing particles[24]).

3.4. Operational characteristics of MWPCs

Since avalanche multiplication occurs in all gases, virtually any gas or gas mixture can be used in a proportional counter. In most cases, however, the specific experimental requirements restrict the choice to several families of compounds; low working voltage, high gain operation, good proportionality, high rate capabilities, long lifetime, fast recovery, etc., are examples of sometimes conflicting requirements. In what follows, we will briefly outline the main properties of different gases in the behaviour of the proportional counter; a more detailed discussion can be found in the bibliography[4–7,12]).

Avalanche multiplication occurs in noble gases at much lower fields than in complex molecules: this is a consequence of the many non-ionizing energy dissipation modes available in polyatomic molecules. Therefore, convenience of operation suggests the use of a noble gas as the main component; addition of other components slightly increases the threshold voltage. The choice within the family of noble gases is then dictated, at least for the detection of minimum ionizing particles, by a high specific ionization and low cost; the choice falls naturally on argon. An argon–operated counter, however, does not allow gains in excess of 10^3–10^4 without entering into a permanent discharge operation; indeed, during the avalanche process, excited and ionized atoms are formed. The excited noble gases can return to the ground state only through a radiative process, resulting in photoelectron extraction from the cathode, which may initiate a new avalanche very soon after the primary.

Argon ions, on the other hand, migrate to the cathodes and are there neutralized extracting an electron; the balance of energy is either radiated as a photon, or by secondary emission, i.e. extraction of another electron from the metal surface. Both processes result in a delayed spurious avalanche: even for moderate gains, the probability of the processes discussed is high enough to induce a permanent régime of discharge.

Polyatomic molecules have a very different behaviour, especially when they contain more than four atoms. The large amount of non-radiative excited states (rotational and vibrational) allows the absorption of photons in a wide energy range. This is a common property of most organic compounds in the hydrocarbon and alcohol families, and of several inorganic compounds like freons, CO_2, BF_3 and others. The molecules dissipate the excess energy either by elastic collisions, or by dissociation into simpler radicals. The same behaviour is observed when a polyatomic ionized molecule neutralizes at the cathode: secondary emission is very unlikely. In the neutralization, radicals recombine either into simpler molecules (dissociation) or forming larger complexes (polymerization). Even small amounts of a polyatomic quencher added to a noble gas change completely the operation of a counter, because of the lower ionization potential that results in a very efficient ion exchange. Good photon absorption and suppression of the secondary emission allows gains in excess of 10^6 to be obtained before discharge.

Unfortunately, the use of polyatomic organic gases can have a dramatic consequence on the lifetime of counters, when high fluxes of radiation are detected. In fact, some products of molecular recombination are liquid or solid polymers. These products deposit on cathodes and anodes, depending on their affinity, and substantially modify the operation of the counter after integral fluxes of radiation around 10^7–10^8 counts per cm^2 when using Isobutane as a quencher[25]). The following process then takes place (Malter effect)[26]): when a thin layer of insulator develops on the cathode, as a result of the deposit of polymers, positive ions created in further avalanches deposit on the outer side of the layer and only slowly leak through the insulator to be neutralized on the cathode. When the detected radiation flux grows above a threshold value (10^2 or 10^3 counts per second per cm^2)

the production rate of the ions exceeds the leakage rate and very quickly a high density of charge develops across the thin layer. The dipole electric field can be so high as to extract electrons from the cathode and through the insulator: a régime of permanent discharge is therefore induced, even if the original source of radiation is removed. Temporary suppression of the counter voltage stops the discharge; the counter, however, remains damaged and an exposure to lower and lower radiation fluxes will start the process again. Only complete cleaning can regenerate a damaged counter.

Fluxes of 10^8 counts per cm^2 are very quickly met in high-energy beams having typical intensities of $10^6/s \cdot cm^2$. A solution to the dilemma has been found by taking advantage of the ion exchange mechanism already mentioned. If a non-polymerizing agent is chosen having its ionization potential lower than those of the other constituents of the gas mixture, addition of even a small quantity of the new quencher will modify the nature of the ions neutralized at the cathode into a non-polymerizing species. Propylic alcohol C_3H_7OH and methylal $(OCH_3)_2CH$ are often used.

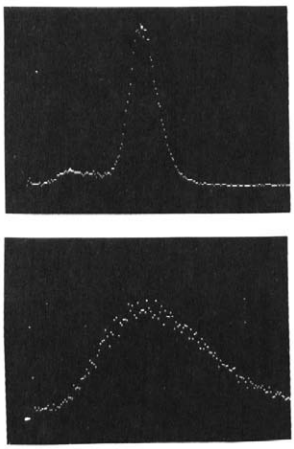

Fig. 11. Pulse-height distribution in the proportional region for ^{55}Fe 5.9 keV X-rays (a) and for minimum ionizing particles (b) in a standard $l=8$ mm, $s=2$ mm wire chamber. The horizontal scale corresponds to about 1 mV/div. (on 1 kΩ) [12].

Integrated rates in excess of 10^{11} counts per cm^2 have been measured, without alteration of the counter properties[25]). Use of organic quenchers with smaller complexity reduces the polymerization[27]), but appears to be less efficient for breakdown protection.

A MWPC operated at moderate gains has a rather good proportional response, as shown in fig. 11, where the actual pulse-height distributions are shown as measured under identical conditions for 5.9 keV X-rays and for minimum ionizing particles in a 16 mm gap chamber, operating with a 60–40 argon–isobutane mixture. In both cases, the horizontal scale is about 1 μA/div. Full efficiency of detection for minimum ionizing particles can be obtained with an electronic threshold around one tenth of the peak amplitude, i.e. about 0.5 mV on 1 kΩ; this is a typically adopted value for operation in the proportional region.

The timing properties of a proportional chamber are determined by the collection time of the electrons produced by the ionizing tracks; the peculiar structure of the electric field around the wires allows the separation of three regions, indicated as A, B, and C in fig. 12. Electrons produced in region A are quickly collected (typical drift velocities in this region of high fields are above 5 cm/μs); tracks crossing the low field region B, however, will produce a characteristic tail in the time distribution. Electrons produced in region C, on the other hand, smoothly drift to the anode where they are amplified and collected. The time resolution of a chamber is defined as the minimum gate width necessary on the detection electronics for full efficiency; it is of around 30 ns for a 2 mm spacing chamber. Fig. 13 shows the typical time distribution observed in such a chamber, when all wires are connected together (meaning that each track crosses region A or B of at least one wire), while fig. 14 shows the same spectrum for a single wire and an inclined beam: the long uniform tail

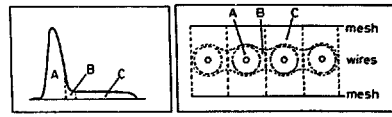

Fig. 12. Timing properties of a multiwire proportional chamber. Depending on where the original charge has been deposited, one can distinguish a "fast" region A, a "drift" region C, and an intermediate region B contributing to the tail in the fast region time distribution (see also fig. 2b) [9]).

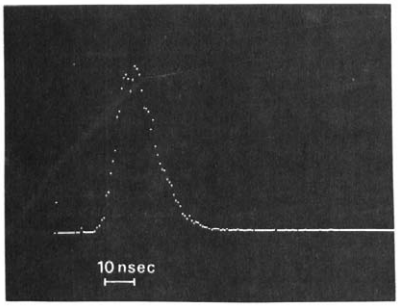

Fig. 13. Typical time distribution measurement in a chamber when all wires are connected together (total OR) [12].

in this case corresponds to tracks crossing region C of the considered wire.

Addition to a proportional gas mixture of small quantities of electronegative vapours, like freon (CF_3Br) [20] or ethyl bromide (C_2H_5) [28] allows the multiplication factor to be pushed to values as high as 10^7 before breakdown, at the same time obtaining a saturated gain condition, i.e. a pulse–height distribution which is entirely independent of the amount of charge lost in the ionizing event. This particular behaviour was extensively studied in the so-called "magic gas"[20], argon–isobutane–freon, in the volume proportions 70–29.6–0.4. The appearance of saturation in these conditions is illustrated by fig. 15, where the

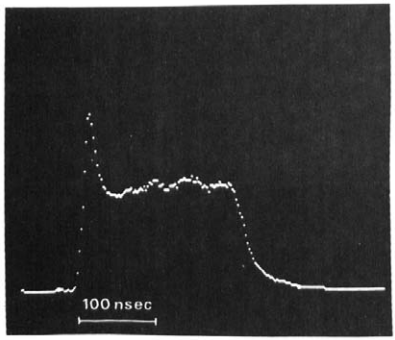

Fig. 14. Typical time distribution measured on a single wire for an inclined beam of minimum ionizing electrons[12].

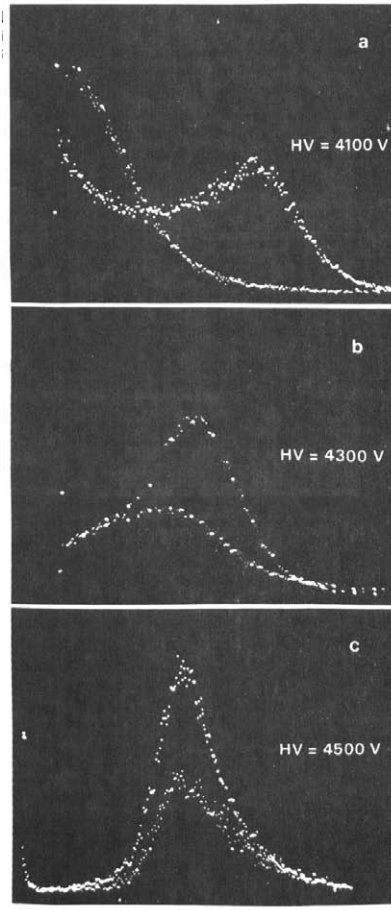

Fig. 15. "Magic gas" operation. Pulse-height spectra measured in a 5 mm gap, 2 mm wire spacing multiwire chamber for ^{55}Fe X-rays and minimum ionizing electrons at increasing anodic voltages, in "magic" gas, showing the pulse-height saturation effect[20]. Notice that the horizontal scales in the three pictures do not coincide (the average pulse height is increasing by more than one order of magnitude from (a) to (c).

pulse-height spectra for minimum ionizing electrons and 5.9 keV photoelectrons are compared at increasingly high operational voltages. In fig. 15a, the amplification is still proportional (the lower peak corresponds to fast electrons), in fig. 15b saturation appears and it is full in fig. 15c. It has been proved that, under these conditions, one single photoelectron provides the full pulse height[29]).

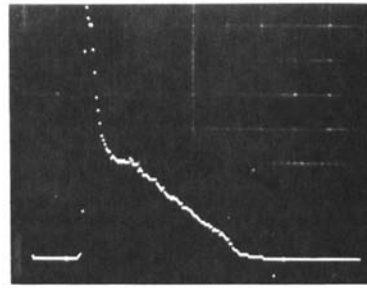

Fig. 16. Time spectrum in a proportional chamber operated with "magic gas", for an inclined charged particle beam. By comparison with fig. 14, one can see the effect of the electronegative vapour addition to the gas in decreasing the effective memory of the chamber[29]).

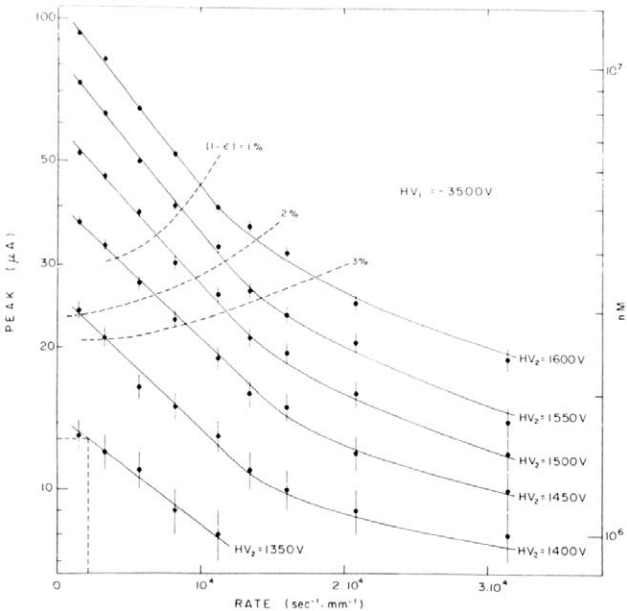

Fig. 17. Space charge effect. When the flux of detected ionizing particles increases, the positive ion charge density in the chamber increases so much as to reduce the electric field around the anode wires and therefore the gain. The curves show the measured peak current for minimum ionizing tracks, at various anodic potentials (or initial gains) as a function of the particle flux. Since the gain reduction appears to be connected to the rate per unit length of the anode wires, the horizontal scale is a linear instead of a surface rate; the real flux is obtained by multiplying the scale by the anode wire spacing. At fixed discrimination threshold on the wire electronics, the efficiency of detection will drop as a consequence of the gain reduction: the dashed curves in the figure show the points of equal inefficiency for a 5 μA threshold[30]).

The amount of electronegative gas that can be used in a chamber is obviously limited by the requirement of full efficiency. An important consequence of the presence of an electronegative gas in the mixture is a reduction of the tail in the time distribution, owing to electron capture, as shown in fig. 16 [29]): the memory of the chamber is therefore correspondingly reduced and this allows operation of the detector at higher particle rates.

There is, however, an intrinsic limitation in the rate capability of MWPCs owing to the formation of a positive space charge by ion produced in the avalanches and migrating to the cathodes. At high enough fluxes, the large positive charge induces a modification of the electric field around the anodes with a consequent reduction of the detected pulse height[30]), as shown in fig. 17; the chamber ceases to be a proportional detector, and even if used only as a digital positioning device efficiency will eventually drop for a fixed electronics detection threshold. A completely new mode of operation has been recently proposed to overcome this fundamental limitation[31]).

4. Methods of read-out

4.1. Anode wires as individual detectors

In most cases, mainly in large detectors, each anode wire is connected to its own circuit and used as an independent detector; the read-out electronics consists essentially of a simple amplifier-discriminator followed by some kind of digitizing system. Several high-density specialized circuits have been developed for this purpose and are available to the experimenter.

If, for tracks perpendicular to the chamber, one expects a single wire to be hit in most of the cases, when detecting inclined tracks, the number of wires hit on each track (or cluster size) will obviously depend on the time gate on the associated electronics. If the gate length is the minimum allowed by the requirement of full efficiency (around 30 ns), the cluster size will be of one or two wires in a ratio depending on the angle; if, on the other hand, the gate length corresponds to the maximum drift-time (about 200 ns for an 8 mm gap), the cluster size will correspond to the maximum allowed by geometry. Fig. 18 shows the measured average cluster size as a function of the angle of incidence of the tracks ($\alpha = 0°$ means tracks perpendicular to the wires plane) for a large

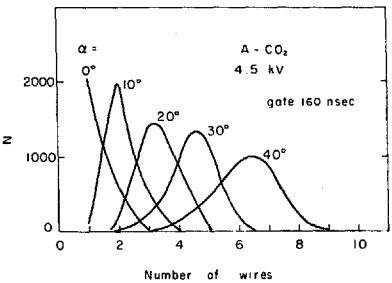

Fig. 18. Distribution of the number of wires hit, or cluster size, in a multiwire proportional chamber operated in standard conditions with a large coincidence gate, for several angles of incidence of the beam[20]).

gate width[20]). A detailed discussion on cluster size and efficiency can be found in Fischer et al.[32]).

When using a gas mixture containing an electronegative vapour, the cluster size is strongly reduced as an effect of electron capture; fig. 19 shows for example how the addition of freon decreases the average number of hit wires, still in the region of full detection efficiency[20]).

4.2. The centre of gravity of cathode induced pulses

We have seen that the precise measurement of induced pulse height distributions in a chamber permits an unambiguous bidimensional response,

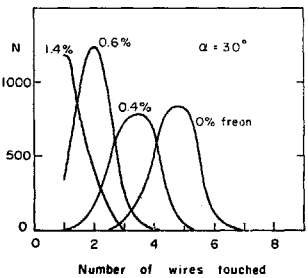

Fig. 19. Distribution of the number of hit wires, for tracks inclined at 30°, as a function of the content of an electronegative vapour (CF_3B_r). Reduction of the sensitive zone around the wires results in a reduced cluster size[20]).

continuous in all directions, with an accuracy close to 50 μm for the best coordinate and 150 μm for the worst.

If a chamber is built with cathodes made of strips, each equipped with an amplifier, a linear delay permitting appropriate logic decisions to be taken and a pulse-height digitizer, localization by computation of the centroid of the induced charges presents the following advantages[21,24]):

– With quite simple amplifiers, the signal-to-noise ratio permits, with a narrow gate of 30–50 ns, accuracies of the order of 50 μm along the wire.

– Such a short gate limits the useful thickness of the chamber to a few millimetres only. Thus, good accuracies can be maintained even for very inclined tracks. If the ionization electrons are shared among several wires the charge centroid gives also an accurate interpolation between wires; with 2 mm wire spacing accuracies of the order of 300 μm between wires have been reached.

– The correlation between the total pulse height induced on the two cathodes, from a given set of avalanches, leads to a partial removal of the ambiguities deriving from the detection of multitrack events. In other words, not only does a single gap provide the track coordinates, but it also serves the purpose reached sometimes by a third chamber set at some angle to the anode wires of two orthogonal chambers, when only the anode wires are being used.

The cost of such a method is too high at present to be envisaged in most large-size detectors. However these unique features of high accuracy two-dimensional detection may make it attractive to solve some particularly difficult experimental problems. For instance a centroid read-out method has been chosen to implement a large size cylindrical detector in a solenoidal field around an intersection of a large electron storage ring[33]).

4.3. Analog read-out methods

Developed at a time when sophisticated electronic circuits for MWPCs were not yet available, analog read-out methods still find applications either if low cost and complexity is of primary concern, or if the chamber geometry does not allow other solutions (like in cylindrical MWPCs). The simplest of them makes use of electromagnetic delay lines, capacitively coupled[34]) to the anode or cathode wire planes (fig. 20); the time difference

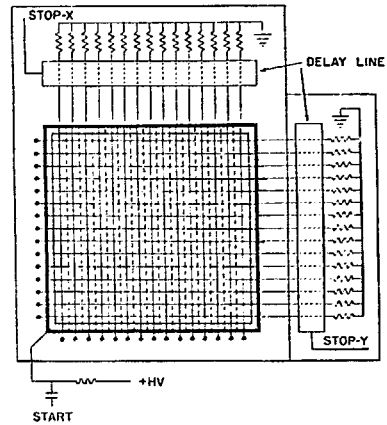

Fig. 20. Coordinate read-out with two electromagnetic delay lines, externally coupled to the cathode wire planes. The time difference between the anode pulse and the two outputs of the delay lines is proportional to the x and y coordinates, respectively[34]).

between the occurrence of the event (as given by an external device or by the anode pulse itself) and the detection of a signal at the ends of the delay line represents the space coordinate.

The use of cathodes made of an insulating foil coated with a high resistance graphite layer permits the collection of the induced pulses on delay lines exterior to the chambers[35]), directly through the cathode planes; this allows selective reading of sections of the chambers. The wires themselves can be connected so as to constitute a delay line[36,37]), or specially built miniature lines can replace some of the cathode wires for direct pick-up of the induced signals[38–40]).

Delay line chambers are simple to make. They provide one of the easiest way to make cylindrical drift chambers[41]). Their use is restricted, however, to applications where the intrinsic good time resolution of the chamber is not essential, since they have a time resolution equal to the total propagation time, usually of several microseconds.

Localization of an avalanche along the anode wires can be obtained also by a charge division method (fig. 21). The problems encountered in this

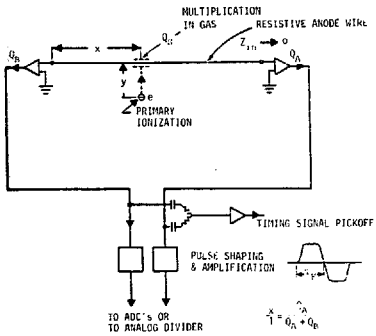

Fig. 21. Localization of the avalanche coordinates using the charge division method. In a resistive wire, the ratio of charges detected at the two ends is proportional to the coordinate along the wire. The time pickoff output can be used for fast coincidence selection or, in a drift chamber, to determine the second coordinate (see the next section)[43]).

technique have been analysed by Radeka et al.[42,43]). The ratio of charges detected at the two sides of a resistive wire is proportional to the coordinate; accuracies of around 0.4% of the wire length have been obtained[44]). Mainly developed to allow the measurement of the coordinate along the axis in cylindrical multiwire chambers, the method is intrinsically bidimensional and allows therefore ambiguity-free reconstruction of high multiplicity.

The choice of a given analog method is sometimes a matter of taste, but is is quite often imposed by physical requirements and represents an adaptation to the physical problems. A good illustration can be found in a special detector for slow neutrons using a pressurized ^{3}He filled chamber[45]). A slow rise-time of the signal, connected to the high pressure operation of the chamber, permits in this case to obtain very good localization with a charge division method, while use of a delay line would lead to very inconvenient rise-time to delay ratios.

On the other hand, delay lines are very practical to read out with a modest accuracy ($\sim$1%) the position of avalanches along the wires of drift chambers with widely spaced anode wires.

It is the art of the experimentalist to choose correctly the best and cheapest read-out adapted to his problem without being embarrassed by the great variety at hand.

5. Drift chambers

5.1. Introduction

A drift chamber is a device in which electrons liberated in a medium by ionizing collisions can be moved away from their initial position by appropriate electric fields and transported to well-determined positions where they are detected.

The most commonly used medium so far has been the gaseous state, although liquid drift chambers merit serious consideration for many applications, since the considerable effort invested during the few years spent in the investigation of the properties of liquefied noble gases as detection media for ionizing particles has shown that they have many properties similar to those of gases[46]).

The displacement of the electrons can serve many purposes:

– If the precise creation time of the initial ionization is known, then the measurement of the time interval between production and detection provides the position of the initial electrons. The importance of drift chambers stems from the fact that, as shown in the very early work on this subject[11]), spatial accuracies of the order of 100 μm and timing accuracies of the order of 5 ns can be achieved by rather simple means. The early application of this technique to various structures showed that a detector[10,47–49]) with considerable potentialities was available.

– The transport of electrons along well-defined lines of force may be used to match a given geometrical situation where one wants all the electrons produced along a line of force to give a unique image; for instance in the spherical drift chambers, where all the electrons produced by soft X-rays along straight lines passing by the centre of a sphere produce a single image[50]).

– Drift spaces may be filled with divided solid matter. The solid is used to give rise to appropriate reactions with charged or neutral particles. The secondaries are detected in the gas in which the matter is embedded: the ionization electrons are milked out from the gas and transferred to a proportional chamber. Efficient detectors for neutral radiations seem feasible[51,52]).

– Large drift volumes offer interesting possibilities. All the information contained in a trajectory,

namely the three-dimensional position of every electron cluster and the energy loss along the track, can be measured after the transfer of the initial electrons to a multiwire chamber. This is the best approximation to a purely electronic track chamber. Considerable effort is being invested in this promising detector under the leadership of Nygren[53]).

Since the laws governing the drift of electron in gases are essential for the understanding and development of drift chambers we will give here a short introduction to this field.

5.2. Drift and diffusion of electrons in gases

The mass of the electrons is so low compared to that of the molecules among which they move that in elastic collisions they retain a large fraction of their momentum. Even in low electric fields the electrons will retain energy gained from the field, and their velocity distribution, which affects their mobility, will be very different from that of the surrounding molecules. This subject is treated in all books related to electrical discharges in gas. It has been reviewed extensively in a recent article by Palladino and Sadoulet[54]) and in the thesis of Schultz[55]).

Since the beginning of the century a great variety of methods have been applied to measure drift velocities. When one now reads the description of different types of electron shutter methods used in this field, one wonders why drift chambers were not invented much earlier, to localize fast particles.

As an example, fig. 22 shows the drift velocity of electrons in some gases. Some salient features of the laws governing the drifting of electrons are the following:

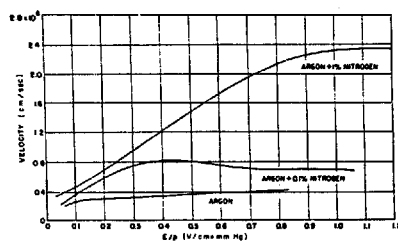

a)

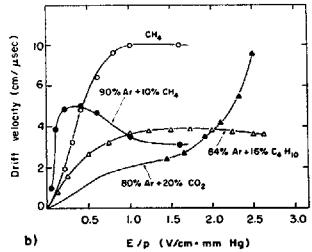

b)

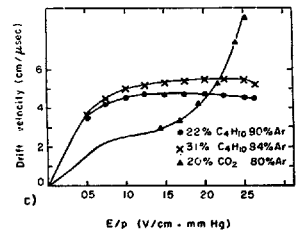

c)

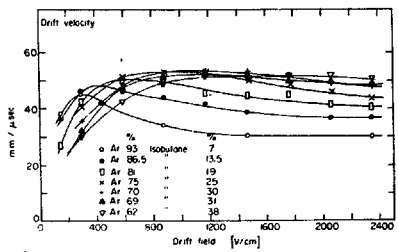

d)

Fig. 22. Examples of drift velocity for electrons in gases, in several mixtures used in proportional counters. The horizontal scale is given either as reduced field E/P, or directly as the field at 1 atm. The drift velocity saturation properties of some gas mixtures are apparent[1,3,30]).

– The drifting in many pure gases is strongly modified by impurities, even in small quantities. The effect is striking in noble gases. The addition of 1% N_2 to argon changes the velocity by a factor of 5 (fig. 22a). In most detectors, complex mixtures are used and the data concerning high-purity gases are of little use.

– The dependence of the drift velocity on the electric field varies widely with the composition of the gas mixtures and their nature (fig. 22b). Very typical in this respect is the case of the Ar–CO_2 and Ar-isobutane mixtures (figs. 22c and d).

In one case the drift velocity is a growing function of the reduced field E/P while in the other case it nearly becomes a constant. The consequence is the different time distribution of the pulses produced in a MWPC filled with these two mixtures. In the first case the distribution is peaked in the short-time region (corresponding to the large fields around the wire) with a long tail in the long-time region (corresponding to the low-field region between the wires). In the second case, it is an almost rectangular distribution with sharp edges, corresponding to the nearly constant drift velocity.

In the drift chambers, where the aim is to measure the position of a particle from the time of drift of the electrons to the sense wires, it is clear that one has to find gases where the velocity is independent of the electric field, unless the measurements are limited to a region of constant field.

Depending on the structure of the chamber and the accuracy, this requirement is more or less stringent.

During the drift in electric field, electrons diffuse following a Gaussian distribution; the change in the energy distribution due to the electric field does, of course, result in a coefficient of diffusion dependent on E.

The r.m.s. of the distribution can be written as:

$$\sigma_x = \sqrt{\left(\frac{2\varepsilon_k}{e}\frac{x}{E}\right)}\frac{1}{\sqrt{P}},$$

where ε_k is the characteristic energy of the electron swarm in the field E, a the gas pressure P, and x is the distance of drift. The expression allows inference of the main characteristics of the electron diffusion, since ε_k is experimentally known for most pure gases, and straighforward formulations allow computation of its value for gas mixtures[54,55]). As an example, fig. 23 shows the dependence of the characteristic energy on the electric field for several argon–isobutane mixtures (a) and for several other gases (b). Increase of the gas pressure, at a constant value of E/P so as to preserve the value of the drift velocity, decreases the diffusion, as is apparent from the quoted expression.

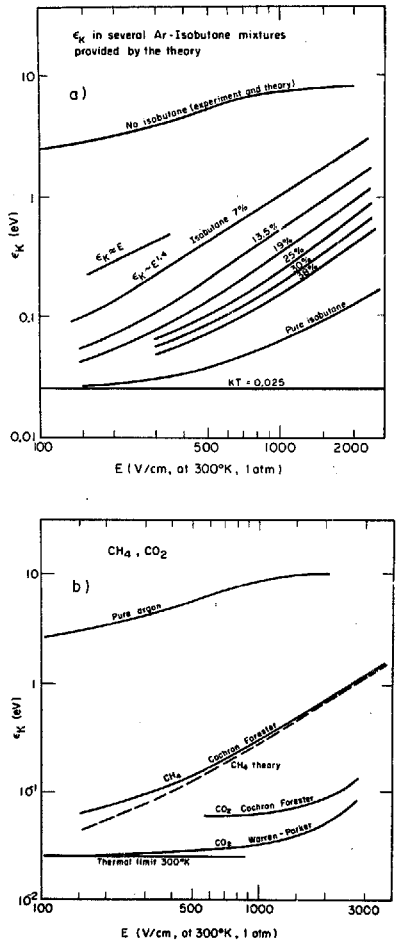

Fig. 23. Characteristic energy of electrons in several gases and gas mixtures, as a function of the electric field. Since the electron space diffusion depends on the square root of ε_k, the choice of a gas with a small characteristic energy is essential in a drift chamber if high localization accuracy is desired[54]).

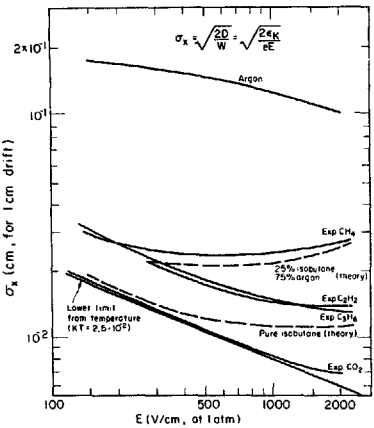

Fig. 24. Computed and experimental dependence of the standard deviation of electron diffusion from the electric field for 1 cm drift, in several gases at normal conditions[54]).

Fig. 24 gives, as a function of the electric field, the computed value of the standard deviation of space diffusion σ_x, for 1 cm of drift. The thermal limit is also shown, corresponding to a fictitious gas where the energy of electrons is not increased by the presence of the field; carbon dioxide, because of its very low characteristic energy, is very close to the thermal limit. For a 75–25 mixture of argon–isobutane, often used in proportional and drift chambers, $\sigma_x \simeq 200\,\mu$m independently of E. In drift chambers, one obtains the space coordinates of ionizing tracks from the measurement of the drift-time, in a more or less uniform field, of the electron swarm. A small diffusion coefficient leads of course to a better accuracy; the choice of carbon dioxide is, however, often forbidden by the poor quenching properties of this gas in proportional counters and the quoted argon-isobutane mixture is preferred.

Notice that the limiting accuracy with which one can localize the drifting swarm is not directly given by σ_x, but by its variance, depending on the number of electrons necessary to trigger the time-measuring device. For example, if the average

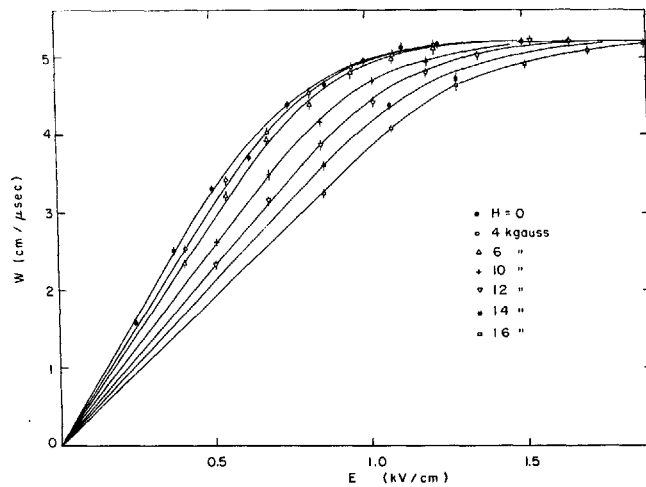

Fig. 25. Measured drift velocity of electrons, along the direction of drift, as a function of the electric field for several values of magnetic field H (perpendicular to E). Curves of this kind depend of course on the gas mixture used, in this case argon–isobutane–methylal (67.2–30.3–2.5) [30]).

time of the n drifting electrons is measured, the limiting accuracy will be $\sigma_x/\sqrt{n}$; on the other hand, if a simple threshold discriminator is used, sensitive essentially to a single electron avalanche, one expects to find a limiting accuracy given by $\sigma_1 \simeq (\ln n)^{-1}\sigma_x$ [54-56]).

The presence of an external magnetic field strongly modifies the drift and diffusion properties of electrons; this point has been carefully investigated since drift chambers are often operated inside large spectrometer magnets. In very first approximation, if $w_0 = w_0(E/P)$ is the drift velocity in the absence of magnetic field, when applying a field $\boldsymbol{H}$ perpendicular to $\boldsymbol{E}$, the new value of the drift velocity is given by[2,54])

$$w_H = w_0 \frac{1}{\sqrt{[1 + (fw_0)^2]}}, \qquad f = \frac{3}{2}\frac{H}{E},$$

and the electron swarm drifts at an angle θ in respect to the electric field direction, as given by $\operatorname{tg}\theta = w_0$. Therefore, when increasing the gas pressure at a constant value of E/P, the tangent of the drift angle is correspondingly reduced.

It appears, however, that such a simple formulation only allows a qualitative estimate of the effect of very high magnetic fields in the testa region. More sophisticated methods of calculation exist in the framework of the quoted theory of electron transport in gases[54,55]); in many cases, however, a direct experimental measurement of the effect may be necessary. As an example, figs. 25 and 26 show, respectively, the measured drift velocity and angle as a function of perpendicular electric and magnetic field, for an argon–isobutane–methylal gas mixture used in high accuracy drift chambers[30]).

A magnetic field does modify also the diffusion properties of electrons; a very strong reduction of the transverse diffusion has been measured in the case where electric and magnetic field are parallel[53]), and this property greatly improves the space accuracy in three-dimensional drift chambers.

5.3. Drift-chamber geometry

In its basic form, a single-cell drift chamber consists of a region of moderate electric field, fol-

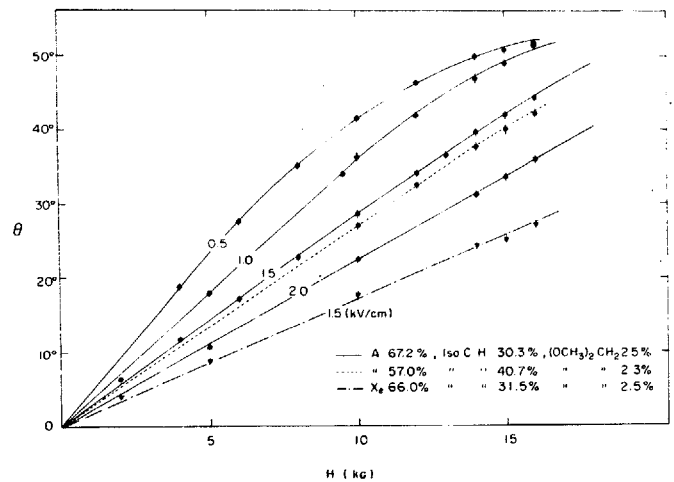

Fig. 26. Measured drift angle, i.e. the angle between electric field and drift direction, as a function of electric and magnetic fields, for several gas mixtures as indicated. The magnetic field direction is perpendicular to E. An increase in the gas density reduces the drift angle, at a given value of electric and magnetic fields[30]).

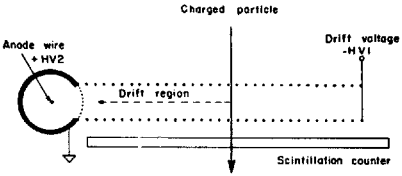

Fig. 27. Principle of operation of a single-cell drift chamber. A set of cathode wires, at suitable potentials, generate in the drift space a region of uniform field. The electrons produced by an ionizing event migrate to one end of the cell[12]).

lowed by a proportional counter (fig. 27). Suitable field shaping electrodes, wires or strips, as shown in the figure, allow one to obtain the desired electrical configuration. Electrons produced at time t_0 by the incoming charged particle migrate against the electric field with velocity w, and reach the anode wire where avalanche multiplication occurs at a time t_1. The coordinate of the track, in respect to the anode wire, is therefore given by

$$x = \int_{t_0}^{t_1} w \, dt,$$

which reduces, for a constant drift velocity, to $x=(t_1-t_0)w$. It is obviously very convenient to have a linear space–time relationship, and this can be obtained in structures with uniform electric field. If a large surface of detection is required, however, a simple structure like the one shown leads to unconfortably large working voltages and very long drift times; nevertheless, chambers of this kind having as much as 50 cm drift lengths have been operated, with an over-all drift voltage around 50 kV and maximum drift-time (or memory) of 7 $\mu\sigma$. The construction of a large 1 GeV spectrometer equipped with such chambers had been undertaken in 1969 and resulted in a remarkably simple detection system[47]). For even larger surfaces, or in cases where shorter memory times are necessary because of the expected particle rates, a multicell structure can be used; in this case, since the region of the anode wire becomes necessarily part of the active volume, it is not possible to obtain a constant drift field all across the cell.

In principle, a structure identical to that of a MWPC can be used to realize a multiwire drift chamber; however, the low-field region between

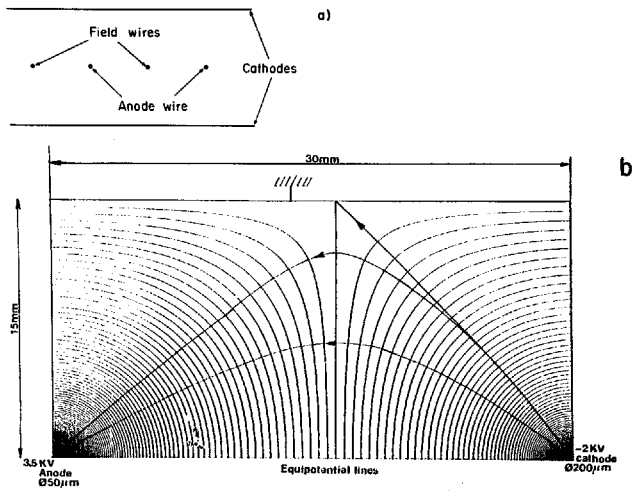

Fig. 28. Principle of the multiwire drift chambers with uniform cathode planes: (a) the basic geometry and (b) the electric field equipotentials in a chamber having 30 mm gap and 60 mm between anode wires[57]).

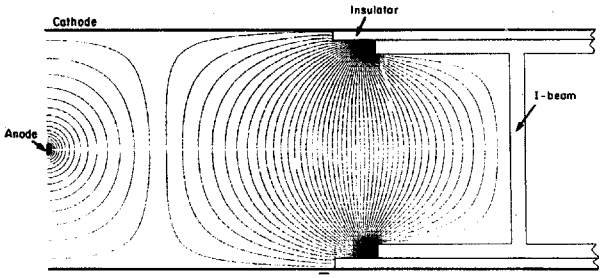

Fig. 29. Equipotentials computed in the Harvard-MIT drift chambers. The field wire has been replaced by an I-shaped profile, insulated from the cathode planes, and serving both the purpose of field reinforcing element and of mechanical stiffener. The gap is 26 mm, the anode wire spacing about 10 cm [59]).

the anode wires would result in a strong non-linearity of the space–time relationship, especially for large wire spacings. A modification of the original proportional chamber structure allows the elimination of low field regions in the central plane[48]). The anode wires are alternated with thick field-shaping cathode wires that reinforce the electric field in the critical regions, as shown in fig. 28 [57]). Chambers of this kind have been built, with wider wire spacings, up to sizes of about 4×4 m^2 [58]). Other designs, similar in principle to the one described, have been developed, which allow a simpler construction of large surface, mechanically very stiff, drift chambers; fig. 29 shows one example[59]). Thin aluminium profiles (I-beam), insulated from the cathode planes and kept at a negative potential, serve both the purpose of mechanical spacers and field-reinforcing electrodes. The cathodes are grounded, while the anode wires are maintained at a positive potential to collect and amplify the electrons.

The major limitation of the structures represented lies in the fact that, in order to obtain a relatively uniform drift field, the ratio of the gap length to the wire spacing has to be maintained close to unity. For typical convenient wire spacings (5–10 cm) this implies rather thick chambers, and therefore a reduced packaging density. Moreover, it takes a long time to collect at the anode all the electrons produced by a track, and therefore multitrack capability per wire is excluded. These considerations have led to the development of the structure shown in fig. 30 [49]). Two sets of parallel cathode wires are connected to increasingly high negative potentials on both sides starting from the centre of a basic cell; the anode wire is maintained at a positive potential, and two field wires, at the potential of the adjacent cathode wires, sharpen the transition from one cell to the next. The equipotential lines are shown on the figure, for a typical choice of operational voltages; a uniform field drift region is produced in most of the

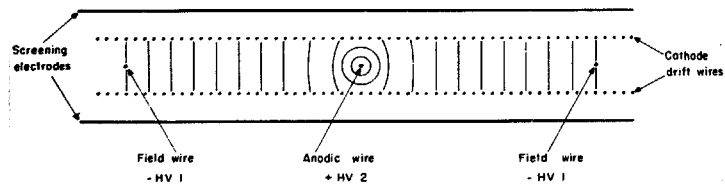

Fig. 30. Principle of construction of the adjustable field multiwire drift chambers. Cathode wires are connected to uniformly decreasing potentials, starting from ground in front of the anode. Field wires reinforce the field in the transition region to the next cell[30,49]).

cell. Small gap-to-anode wire spacing ratios can therefore be implemented; typical values of 6 mm and 50 mm have been used for the gap and the anode spacing, respectively. Notice that since the cathode planes are not equipotential, some field lines escape from the structure; subsidiary grounded screening electrodes, as shown in the figure, guarantee the immunity of the drift field from external perturbations.

Other structures have been developed, mainly in the field of very large size detectors.

In a large neutrino detector at CERN, drift chambers of 4.5 m × 4.5 m use uniform cathodes with the addition of several field shaping wires[57]). In a large magnetic cylindrical detector, extremely simple layers of drift cells are used, consisting of three field wires on each side of an anode wire. A small angle between the direction of the wires in successive layers permits a two-dimensional readout of a track[60]).

5.4. Positioning accuracy and time measurements

The ultimate accuracy that can be obtained in a drift chamber depends both on the good knowledge of the space–time relationship and on the diffusion properties of electrons in gases. From the previous considerations it appears that, for most gases commonly used in proportional counters, intrinsic accuracies (due to diffusion) below 100 μm are possible for minimum ionizing particles. The space–time correlation, however, may not be known at this level of accuracy, especially for large chambers where various mechanical tolerances can locally modify the electric field structure. Very good results in terms of stability of operation and

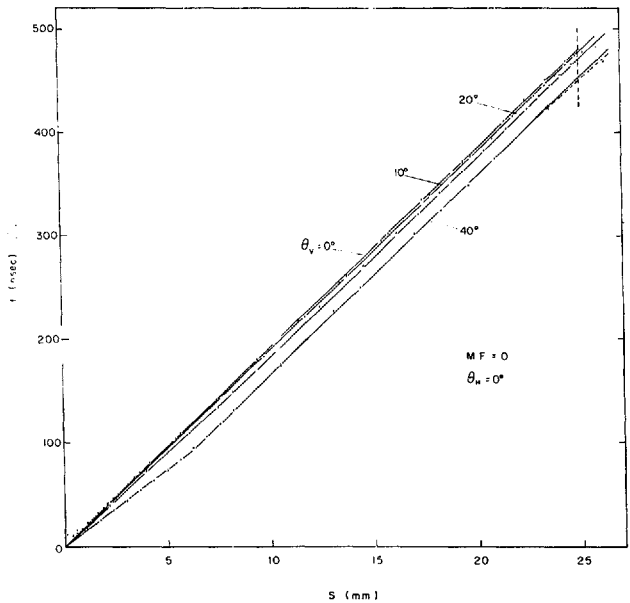

Fig. 31. Measured and computed space–time relationship for the chamber in fig. 30, as a function of the minimum ionizing beam angle of incidence[30]).

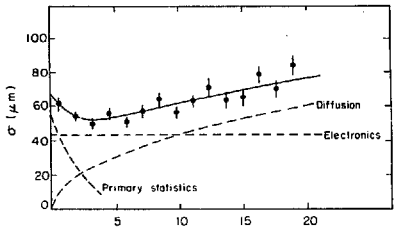

Fig. 32. Measured intrinsic accuracy in the drift chamber of fig. 30, as a function of drift space. The experimental results have been decomposed into three contributions: a constant electronics dispersion, a physical diffusion term function of the square root of the drift space, and a contribution of the primary ion pair statistics[61,56]).

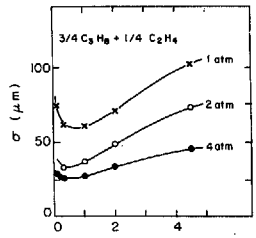

Fig. 33. Measured dependence of the accuracy of localization in a drift chamber on the gas pressure. Increase in p results both in a decrease in electron diffusion, and in a reduction in the primary ion pair statistics effect, because of the increase in the specific ionization[16]).

reproducibility have been obtained combining the good electric field characteristics of the structure shown in fig. 30 and the saturated drift velocity peculiarity obtained in selected gas mixtures.

In these conditions, space–time relationships like the ones shown in fig. 31 are obtained; for tracks perpendicular to the chamber, the correlation is strictly linear within the measurement errors.

In a structure where the electric field is less uniform, the space–time relationship is obviously more or less deviating from linearity especially if some regions of field are low enough not to allow drift velocity saturation.

The intrinsic accuracy of a chamber can be estimated by the usual method of measuring the same track in a set of equal chambers, and computing the standard deviation of the difference, in a given chamber, between the measured and the fitted coordinate. A typical experimental result is presented in fig. 32[61]), which gives the accuracy as a function of the drift distance in a chamber like the one in fig. 30. The result can be decomposed into three main contributions: a square root dependence on the distance of drift due to electron diffusion; a constant electronics spread estimated to correspond to about 40 μm as from the figure; and a contribution of the primary electrons' production statistics, particularly important close to the anode wire[56]).

As shown explicitly in the expression giving the r.m.s. of electron diffusion (section 5.2), operation at high pressures improves the space accuracy, as shown in fig. 33 [16]).

As far as the proportional gain is concerned, drift chambers are, in general, easier to operate than MWPCs, being essentially isolated proportional counters; all considerations on multiplication factors and gas choice apply as well, with the necessary modifications due to the geometry. Common practice has shown that commercial grade purities are sufficiently good for moderate drift lengths (a few cm), but that the gas tightness of the chamber and of the tubing has to be carefully checked. In some cases, a gas monitoring device at the output of a chamber or a chamber system is advisable.

It should be emphasized that the intrinsic accuracy given in fig. 32 is the result of a local measurement, normally realized in a short run and essentially independent of the detailed space–time correlation. To make use of the quoted accuracies in an actual coordinate measurement, one has, of course, to know precisely the space–time correlation or the drift velocity $w = w(t)$. For a given chamber geometry, the major factors that can influence the drift velocity are: the electric field strength and direction, the atmospheric pressure, the gas composition and temperature, the presence of external factors modifying the drift properties (electric or magnetic stray fields), and the mechanical imperfections. Although it is, in principle, possible to take all these factors into account by proper calibration or monitoring, for a realistic system it is more reasonable to set definite limits to the tolerable variations, as a function of the desired final accuracy. The choice of a drift-velocity saturating gas obviously decreases or eliminates

the dependence on the reduced electric field E/P. It appears also[55]) that for several gases and gas mixtures the temperature dependence of w is reduced at high fields; for the particular mixture used by the authors of ref. 30 the calculation gives a value very close to the experimentally measured one, i.e. $\Delta w/w = 3 \times 10^{-4}$ per °C at a field around 1.4 kV/cm. At low fields, and for the same mixture, the relative variation is about one order of magnitude larger. The dependence on gas composition also reduces at saturation, and has been measured in the quoted gas mixture to be $\Delta w/w = 1.2 \times 10^{-3}$ for 1% change in the gas.

If the position of a particle is known, then the space–time correlation yields the time of creation of the ionizing trail. In the drift chambers with adjustable field, the spatial accuracy of 100 μm corresponds to a timing accuracy of 2 ns. Now, the best way to obtain the position is also to use drift chambers. If the particles come from a given direction, one single additional drift chamber is sufficient, provided the zero time is given by a scintillator. In this case, one does not really need the additional drift chamber in order to know the time. It has only the virtue of giving a second piece of time information that permits the rejection of particles accidentally crossing the chambers while the electrons corresponding to the event tagged by the scintillator are drifting. From the point of view of accidentals, two drift chambers in series thus correspond to a very sharp detector with 5 ns resolution. An example of such use was given by Heintze and Walenta[62]) with proportional chambers with wires spaced every 5 mm. They reported an accuracy of 6 ns (FWHM), which has to be tempered by the fact that as the response is not Gaussian (to be expected with an inhomogeneous chamber) the real resolution time for 100% efficiency is close to 25 ns.

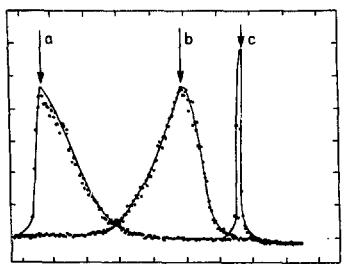

Fig. 34. Time resolution of staggered drift chambers. The picture shows the time distributions a and b of two chambers in a narrow beam; the wire spacing is 5 cm. The two chambers are staggered by half a wire spacing in a magnetic field of 18 kG (the horizontal scale is 100 ns/div.). The peak c is the distribution of the sum of the drift times, $T_1 + T_2$, obtained by simple hardware means (fwhm ≃ 2 ns). We see that two such chambers define the time of passage of the particle with a very good accuracy.

Fig. 34 shows the resolution obtained with two staggered chambers, 2 m × 2 m, with a wire spacing of 5 cm in a magnetic field of 18 kG[63]). If the two chambers are staggered by half a wire spacing, one has the additional advantage of resolving the right–left ambiguity which plagues multiwire drift chambers.

If, however, two drift chambers are used to measure the position by measuring the difference in the detection time between two staggered chambers, then the third one gives the time. With the measured time accuracies for each drift time, one may expect to define the time reference to within about 4 ns. It is also possible with three such chambers to select a given sagitta in a magnetic field, thus permitting a rapid momentum selection. Again, with the measured average 100 μm accuracy per chamber, with three chambers 10 cm apart, a 1 GeV/c momentum should be measured to about 2%.

5.5. The three-dimensional drift chamber

In some problems encountered in high-energy physics a continuous sampling of particle trajectories is necessary. Not only the coordinates but also the energy losses are required for the interpretation of very complex trajectory configurations and particle identification.

Recently, a new approach to the detection problem has appeared, with the introduction of large-volume drift chambers such as the ISIS detector[64]), the time projection chamber[53]) and similar devices[65–67]).

These detectors consist essentially of a large gas container, constituting the sensitive volume, in which the electrons produced by the ionizing tracks drift along a suitable electric field to an end-cap MWPC; through avalanche multiplication the charges are amplified there to allow electronic detection. As can be seen from fig. 35 the cathode plane C1 is built with a wire mesh or a grid having good electrical transparency for the drifting

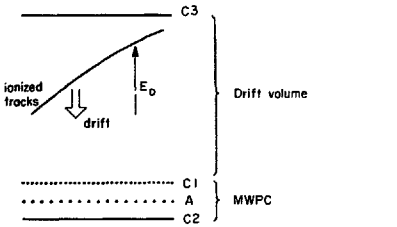

Fig. 35. Volume drift chamber or time projection chamber. Electrons produced by ionizing track in a large gas volume drift to and end-cap multiwire proportional chamber where they are detected. Storage and subsequent analysis of the amplitude detected on anode and cathode wires as a function of time allows a full three-dimensional reconstruction of complex events.

electrons, while cathode C2 can be a conducting foil or a printed circuit suitably stripped to provide a coordinate measurement. The anode plane A can either be constituted by a single mesh of thin wires, or by an alternation of thin (anode) and thick (field) wires. Suitable guard rings (not represented in the figure) on the periphery of the drift volume, maintain the uniformity of the applied drift field E_D over all the sensitive volume.

In the time projection chamber detector (fig. 36) the event topology sliced in narrow time intervals (hence the name of the detector) is rapidly stored in a large system of analogue shift registers that are then multiplexed and read out at a conveniently lower speed. The order number of the considered time slice, as referred to the event time, gives the elevation of each projection, while the anodic wire number and the induced pulse-height distribution on cathode strips or pads gives the two-dimensional coordinates of each segment in the projection; the anode pulse height is considered to represent the energy deposit of the corresponding track segment. The whole detector, cylindrical in shape, is immersed in a solenoidal magnet such that the electric and magnetic fields are parallel: the drift direction of electrons is therefore not modified and, as mentioned in section 5.4, their transverse diffusion is strongly reduced.

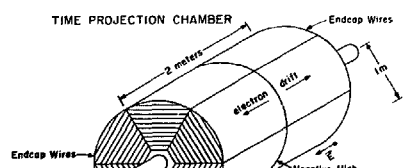

Fig. 36. The time projection chamber. It has a cylindrical shape, so as to fit inside a large solenoid magnet. Two independent drift volumes terminate with an end-cap multiwire proportional chamber where both time and energy loss information is extracted. The structure operated at a high gas pressure (10 atm) to improve energy resolution[53]).

Although the development of such detectors seems promising, several less ambitious approaches have been undertaken in several laboratories dealing with the same problem. In most cases solutions have been adopted where independent drift spaces with two-dimensional read-out based on more conventional approaches like current division are used for the sampling of the trajectories[44,66]).

We should also mention that serious doubts have been cast on the possibility of using large volume drift chambers in high flux condition, because of the deleterious effects of positive ion space charge on the drift properties[68]).

References

1) S. C. Brown, *Basic data of plasma physics* (Wiley, New York, 1959).
2) L. B. Loeb, *Basic processes of gaseous electronics* (University of California Press, Berkeley, 1961).
3) L. G. Christophorou, *Atomic and molecular radiation physics* (Wiley, New York, 1971).
4) S. A. Korff, *Electron and nuclear counters* (Van Nostrand, New York, 1955).
5) W. Franzen and L. W. Cochran, in *Nuclear instruments and their uses* (ed. A. H. Snell; Wiley, New York, 1956).
6) S. C. Curran and J. D. Craggs, *Counting tubes, theory and applications* (Butterworths, London, 1949).
7) P. Rice-Evans, *Spark, streamer, proportional and drift chambers* (Richelieu, London).
8) G. Charpak, R. Bouclier, T. Bressani, J. Favier and C. Zupancic, Nucl. Instr. and Meth. 62 (1968) 235.
9) G. Charpak, Ann. Rev. Nucl. Sci. 20 (1970) 195.
10) G. Charpak, D. Rahm and M. Steiner, Nucl. Instr. and Meth. 80 (1970) 13.
11) G. Charpak, J. Phys. 30 (1969) 86 C2.
12) F. Sauli, CERN 77-09 (1977).
13) G. Charpak, Nucl. Instr. and Meth. 156 (1978) 1.
14) G. A. Erskine, Nucl. Instr. and Meth. 105 (1972) 565.
15) E. Mathieson, T. J. Harris, Nucl. Instr. and Meth. 154 (1978) 189.
16) W. Farr, J. Heintze, K. H. Hellenbrandt and A. H. Walenta, Nucl. Instr. and Meth. 154 (1978) 175.

17) A. Breskin, Nucl. Instr. and Meth. **141** (1977) 505.
18) G. Charpak, G. Petersen, A. Policarpo and F. Sauli, IEEE Trans. Nucl. Sci. NS-25 (1978) 122.
19) J. Fischer, M. Okuno and A. H. Walenta, Nucl. Instr. and Meth. 151 (1978) 451.
20) R. Bouclier, G. Charpak, Z. Dimcowski, G. Fischer, F. Sauli, G. Coignet and G. Flügge, Nucl. Instr. and Meth. 88 (1970) 149.
21) G. Charpak, G. Petersen, A. Policarpo and F. Sauli, Nucl. Instr. and Meth. 148 (1978) 471.
22) S. Brehin, A. Diamant Berger, G. Marel, G. Tarte, R. Turlay, G. Charpak and F. Sauli, Nucl. Instr. and Meth. 123 (1975) 225.
23) C. Charpak and F. Sauli, Nucl. Instr. and Meth. 113 (1973) 381.
24) G. Charpak, G. Melchart, G. Petersen and F. Sauli, High accuracy localization of minimum ionizing particles, to be published in Nucl. Instr. and Meth.
25) G. Charpak, H. G. Fischer, C. R. Grühn, A. Minten, F. Sauli, G. Plch and G. Flügge, Nucl. Instr. and Meth. 99 (1972) 279.
26) L. Malter, Phys. Rev. 50 (1936) 48.
27) D. Friedrich and F. Sauli, CERN EP Internal Report 77-10 (1977).
28) G. Grunberg, L. Cohen and L. Mathieu, Nucl. Instr. and Meth. 78 (1970) 102.
29) M. Breidenbach, F. Sauli and R. Tirler, Nucl. Instr. and Meth. 108 (1973) 23.
30) A. Breskin, G. Charpak, F. Sauli, M. Atkinson and G. Schultz, Nucl. Instr. and Meth. 124 (1975) 189.
31) G. Charpak, G. Melchart, G. Petersen, F. Sauli, E. Bourdinaud, B. Blumenfeld, C. Duchazeaubeneix, A. Garin, S. Majewski and R. Walczak, CERN 78-05 (1978).
32) H. Fischer, F. Piuz, W. G. Schwille, G. Sinapsius and O. Ullaland, Proc. Int. Meeting on *Proportional and drift chambers*, Dubna (1975) p. 158.
33) J. Davier et al., Laboratoire de l'Accélérateur linéaire, in preparation.
34) R. Grove, K. Lee, V. Perez-Mendez and J. Sperinde, Nucl. Instr. and Meth. 89 (1970) 257.
35) H. Okuno, R. L. Chase, J. Fischer and A. H. Walenta, IEEE Trans. Nucl. Sci. NS-24 (1971) 213.
36) G. Charpak, R. Bouclier, T. Bressani, J. Favier and C. Zupancic, Nucl. Instr. and Meth. 65 (1968) 217.
37) D. M. Lee, J. E. Sobottka and H. A. Thiessen, Los Alamos Report LA-4968-MS (1972).
38) G. Charpak, Proc. Int. Conf. on *Instrumentation for high-energy physics*, Frascati (1973).
39) A. Breskin, G. Charpak, B. Gabioud, F. Sauli, N. Trauntner, W. Duinker and G. Schultz, Nucl. Instr. and Meth. 119 (1974) 9.
40) M. Atac and W. E. Taylor, Nucl. Instr. and Meth. 120 (1974) 147.
41) L. Camilleri et al., Nucl. Instr. and Meth. 156 (1978) 275.
42) V. Radeka, IEEE Trans. Nucl. Sci. NS-21 (1974) 51.
43) V. Radeka and P. Rehak, IEEE Trans. Nucl. Sci. NS-25 (1978).
44) C. W. Fabjan, J. Lindsay, F. Piuz, F. Ranjard, E. Rosso, A. Rudge, S. Serednyakov, W. T. Willis, H. B. Jensen and J. D. Petersen, Nucl. Instr. and Meth. 156 (1978) 267.
45) J. Alberi, J. Fisher, V. Radeka, L. C. Rogers and B. Schoenborn, BNL 19487 (1975).
46) H. H. Chen and J. F. Lathrop, Nucl. Instr. and Meth. 150 (1978) 585.
47) J. Saudinos, in Proc. Topical Seminar on *Interactions of elementary particles with nuclei*, Trieste, 1970 (INFN, Trieste); J. Saudinos, J. C. Duchazeaubeneix, C. Laspalles and R. Chaminade, Nucl. Instr. and Meth. 111 (1973) 77.
48) A. H. Walenta, J. Heintze and B. Schürlein, Nucl. Instr. and Meth. 92 (1971) 373.
49) G. Charpak, F. Sauli and W. Duinker, Nucl. Instr. and Meth. 108 (1973) 413.
50) G. Charpak, C. Demierre, R. Kahn, J. C. Santiard and F. Sauli, Nucl. Instr. and Meth. 141 (1977) 449.
51) A. P. Jeavons, D. W. Townsend, N. L. Ford, K. Kull, A. Manuel, O. Fischer and M. Peter, CERN DD Internal Report 77-15 (1977).
52) C. B. Lim, D. Chu, L. Kaufman, V. Perez-Mendez, R. Hattner and D. C. Price, IEEE Trans. Nucl. Sci. NS-22 (1975) 388.
53) Proposal for a PEP Facility based on the Time Projection Chamber (PEP 4, Dec. 1976), Spokesman: D. Nygren.
54) V. Palladino and B. Sadoulet, Nucl. Instr. and Meth. 128 (1975) 323.
55) G. Schultz and J. Gresser, Nucl. Instr. and Meth. 151 (1978) 413.
56) F. Sauli, Nucl. Instr. and Meth. 156 (1978) 147.
57) G. Marel, P. Bloch, S. Brehin, B. Devaux, A. M. Diamant-Berger, C. Leschevin, J. Maillard, Y. Malbequi, H. Martin, A. Patoux, J. Pelle, J. Plancoulaine, G. Tarte and R. Turlay, Nucl. Instr. and Meth. 141 (1977) 43.
58) D. C. Cheng, W. A. Kozanecki, R. L. Piccioni, C. Rubbia, R. L. Sulak, H. J. Weedon and J. Wittaker, Nucl. Instr. and Meth. 117 (1974) 157.
59) Experiment R209 at CERN (H. Newman, private communication).
60) W. Davies-White et al., SLAC-PUB-2181 (1978).
61) N. A. Filatova, T. S. Nigmanov, V. P. Pugachevich, V. D. Riabtsov, M. D. Shafranov, E. N. Tsyganov, D. V. Uralsky, A. S. Vodopiśnov, F. Sauli and M. Atac, Nucl. Instr. and Meth. 143 (1977) 17.
62) J. Heintze and A. H. Walenta, Nucl. Instr. and Meth. 111 (1973) 461.
63) G. Charpak, ESRO SP-109 (1975), p. 109.
64) W. W. Allison, C. B. Brooks, J. N. Bunch, J. H. Cobb, J. L. Lloyd and R. W. Plenning, Nucl. Instr. and Meth. 119 (1974) 499.
65) W. Bartl et al., PETRA 76/16 (1976).
66) W. Farr, B. Granz, J. Heintze, R. D. Hever, P. Lennert, T. Nozski, A. Rieseberg and A. Wagner, Nucl. Instr. and Meth. 156 (1978) 283.
67) A. Astbury et al., CERN/SPSC/78-06 (1978).
68) D. Freidrich, G. Melchart, B. Sadoulet and F. Sauli, Nucl. Instr. and Meth. 158 (1979) 81.